Journal of Solid State Chemistry 182 (2009) 869–874

Contents lists available at ScienceDirect

Journal of Solid State Chemistry

journal homepage: www.elsevier.com/locate/jssc

The influence of co-doping Ag and Sb on microstructure and thermoelectric properties of PbTe prepared by combining hydrothermal synthesis and melting

H. Li [a], K.F. Cai [a,*], H.F. Wang [a], L. Wang [a], J.L. Yin [b], C.W. Zhou [a]

[a] Tongji University, Functional Materials Research Laboratory, 1239 Siping Road, Shanghai 200092, China
[b] Tongji University, Shanghai Key Laboratory of Development and Application for Metal-Functional Materials, 1239 Siping Road, Shanghai 200092, China

ARTICLE INFO

Article history:
Received 10 September 2008
Received in revised form
12 December 2008
Accepted 18 January 2009
Available online 20 February 2009

Keywords:
PbTe
Doping
Thermoelectric
Semiconductor

ABSTRACT

Ag and Sb co-doped PbTe ($AgPb_{18}SbTe_{20}$) and pure PbTe nanopowders were hydrothermally synthesized. The synthesized nanopowders were heated at 1173–1223 K in vacuum for 5 h followed by a slow cooling. The nanopowders and the bulk samples were characterized by X-ray diffraction and electron microscopy, respectively. Electrical transport properties of the bulk samples were measured from room temperature to ~773 K. The results showed that co-doping Ag and Sb into PbTe has significant effects on both the nanopowders and bulk samples. Bulk $AgPb_{18}SbTe_{20}$ sample showed n-type conduction in the whole temperature range measured, while bulk PbTe sample exhibited a transition from p- to n-type conduction at ~500 K. The thermoelectric properties of PbTe were markedly improved after co-doping of Ag and Sb. The $AgPb_{18}SbTe_{20}$ sample has a dimensionless figure of merit of ~0.94 at 723 K.

1. Introduction

Thermoelectric (TE) materials have attracted renewed interest for their potential applications in future energy production, conversion, management, and utilization [1]. The efficiency of a TE device depends on the TE properties of the materials used. Whereas the effectiveness of a TE material is determined by its dimensionless figure of merit, ZT ($=S^2\sigma T/\kappa$, where T is the absolute temperature, S is the Seebeck coefficient, σ is the electrical conductivity and κ is the thermal conductivity of the material). During the last decade, great efforts have been made on enhancing the ZT values of materials [2–4].

PbTe is a typical TE material functioning in an intermediate temperature range (400–800 K) [5]. Many methods, such as doping [6,7], alloying [8] and grain-size control [9,10] have been tried to improve the TE properties of PbTe materials. In 2004, Kanatzidis group [11] reported that the ZT value of n-type Ag and Sb co-doped PbTe, $AgPb_mSbTe_{2+m}$ or LAST-m (LAST stands for Lead Antimony Silver Tellurium), was extremely high (ZT = 1.7 at 700 K for LAST-18). The LAST-m samples were prepared by heating high-purity elemental Ag, Pb, Sb and Te at 1123 K for 4 h followed by a slow cooling. The high performance of the LAST-m samples was attributed to the formation of endotaxially embedded nanostructures [12]. Many other groups were inspired by the progress and started to study the LAST-m system. For example, Kosuga et al. have done a series of studies on the LAST-m system via hot pressing, using either high-purity elemental Ag, Pb, Sb and Te or tellurides (PbTe, Ag_2Te, Sb_2Te_3) as the starting materials, whereas the best ZT value obtained is about 1.0 at 673 K for a sample of $Ag_{0.6}Pb_{18}SbTe_{20}$ [13]. Li and coworker [14] studied the LAST-m system by combining mechanical alloying and spark plasma sintering (SPS), also using high purity elemental Ag, Pb, Sb and Te as the starting materials. They, however, found that high ZT value could only be obtained when the composition was rich in Pb. Most recently, they reported that the TE properties were significantly improved by a long time annealing after SPS. The ZT value at 700 K for an $Ag_{0.8}Pb_{22.5}SbTe_{20}$ sample was increased from 1.05 before annealing to 1.5 after annealing at 653 K for 30 days in vacuum [15].

Besides the progress in PbTe based system, many other material systems with high ZT values have been reported. However, until now, TE materials have not been extensively used. A key reason is that the cost of the materials is high. As we all know that the high purity elements are very expensive that will increase the cost of the materials. In addition, hot pressing especially SPS will cause the materials much more expensive.

We have recently investigated a low cost method to the LAST-m materials [16]: LAST-m nanopowders are firstly hydrothermally synthesized, using $Pb(NO_3)_2$, $AgNO_3$, $Sb(NO_3)_3$ and Te powder as the starting materials and $NaBH_4$ as a reductant, and

* Corresponding author. Fax: +86 21 65980255.
E-mail addresses: kfcai@tongji.edu.cn, kfcai@mail.tongji.edu.cn (K.F. Cai).

0022-4596/$ - see front matter © 2009 Elsevier Inc. All rights reserved.
doi:10.1016/j.jssc.2009.01.017

then the nanopowders are compacted into pellets via cold pressing, and finally the pellets are pressurelessly sintered in Ar. The materials show large positive Seebeck coefficient but low electrical conductivity, resulting in a relatively low power factor ($S^2\sigma$). This is because on one hand, a small amount of unreacted Te remains in the sintered materials; on the other hand, the nanopowders absorb some air due to high surface area, a small part of which remains inside the pellets, so that the sintered materials are slightly oxidized during the sintering. Both the remnant Te and the introduction of oxygen result in the materials exhibiting p-type conduction [16]. In this work, we used Na_2TeO_3 to replace Te powder for the hydrothermal synthesis. Moreover, for compacting, the hydrothermally synthesized nanopowders were heated in a sealed quartz tube under vacuum. The results showed that this could be a promising route to LAST-*m* materials with high ZT values.

2. Experimental procedure

Analytical purity $Pb(NO_3)_2$, $AgNO_3$, $SbCl_3$, and Na_2TeO_3 were used as the precursors. In a typical synthesis of LAST-18 nanopowders, about 40 mL deionized water was poured into a 100-mL beaker, and the beaker was placed on the plate of a magnetic force stirring device. The above precursors with the stoichiometric ratio of $AgPb_{18}SbTe_{20}$ were placed into the beaker one by one under constant stirring with a magnetic bar; after that, enough KOH and KBH_4 were added into the beaker. The mixture was kept under stirring for 10 min before being poured into a 100-ml Teflon autoclave. Some deionized water was added into the autoclave until ~85% of its volume was filled; subsequently, the autoclave was sealed, then placed into an oven, heated up to 180 °C and held at 180 °C for 20 h, and cooled naturally to room temperature. Black precipitates at the bottom of the autoclave were collected and washed with deionized water and absolute ethanol in sequence for several times, and then separated by centrifugation for 5 min at 4000 rpm. The obtained black product was dried in vacuum at 70 °C for 6 h.

The dried powders were loaded into a graphite crucible and then sealed in a quartz tube under 6.7×10^{-3} Pa before being flushed with argon for several times. The quartz tube was heated to ~1173–1223 K, held at the temperature for 5 h, and then cooled to 723 K in 60 h, followed by naturally cooling to room temperature. Cylinder-like sample was obtained at the bottom of the graphite crucible. For the synthesis of PbTe powders and bulk samples, other conditions were the same as described above except that no salts of Ag and Sb were added during the hydrothermal synthesis process.

The phase composition of the as-prepared nanopowders and bulk samples was examined by X-ray diffraction (XRD, Bruker D8 Advance), with Cu*K*α radiation ($\lambda = 1.5406$ Å). The morphology of the as-prepared powders was observed by means of transmission electron microscopy (TEM, H-800). Scanning electron microscopy (SEM, JEOL JSM5510) was used to observe the fracture surface of the as-prepared bulk samples. The composition of the LAST-18 sample was analyzed by means of X-ray fluorescence spectrometer (XRF, Brucker SRS3400). The bulk samples were cut into pellets (~1 mm in thickness and 10 mm in diameter) and rectangular pieces ($10\times1\times2$ mm^3) for thermal and electrical properties measurement, respectively. Electrical conductivity measurement was performed using a steady-state four-probe technique with chopped direct current (~10 mA), and the Seebeck coefficient was determined by the slope of the linear relationship between the thermoelectromotive force and temperature difference (~10 K) between the two ends of the sample. The Hall coefficient and carrier concentration of the samples were measured at room temperature using HMS-3000 (Ecopia) with a magnetic field of 0.55 T. Thermal conductivity (κ) was calculated using the equation $\kappa = \upsilon C_p d$, where υ is the thermal diffusivity, C_p is the specific heat, and d is density of the sample. The thermal diffusivity was measured from 310 to 723 K on a laser flash apparatus (Netzsch, LFA-457) in Ar, and the specific heat was measured using differential scanning calorimeter (Netzsch, DSC 404) in Ar. The bulk density was determined by the Archimedes method.

3. Results and discussion

Fig. 1(a) shows the XRD patterns for the as-prepared PbTe and LAST-18 powders. It can be seen from Fig. 1(a) that the XRD patterns for the PbTe and LAST-18 powders are quite similar and that all the peaks for both the PbTe and LAST-18 powders can be indexed to the reported data for cubic PbTe (JCPDS card, no. 77-0246), which is also given in Fig. 1(a) for comparison. This indicates that pure products have been obtained. Figs. 1(b) and (c) show typical TEM images for the as-prepared PbTe and LAST-18 powders, respectively. Both the powders consist of cubic nanoparticles with sizes in range of ~65–150 and ~40–95 nm, respectively. Obviously, the Ag and Sb co-doping decreases the particle size of the synthesized powder. The selected area electron diffraction (SAED) patterns (insets in Figs. 1(b) and (c)) reveal that both the nanopowders are crystalline. It is calculated from the SAED patterns that the unit cell parameter for the PbTe and the LAST-18 powders is 0.6478 and 0.6454 nm, respectively, indicating that the unit cell parameter of PbTe decreases after co-doped with Ag and Sb. This trend is in agreement with the result reported in Ref. [11].

XRD patterns of the bulk PbTe and LAST-18 samples are shown in Fig. 2(a). All the peaks can be indexed to cubic PbTe. It can be seen from Fig. 2(a) that the peak intensities of XRD patterns for the PbTe and the LAST-18 samples are quite different. Both the samples have a preferential crystallographic orientation and the preferential orientation for the PbTe and LAST-18 samples is [110] and [100], respectively. Such preferential orientations in the LAST-*m* samples have not been reported yet.

Figs. 2(b) and (d) are typical SEM images, at low magnification, of the fracture surface of the PbTe and LAST-18 samples, respectively, revealing that both the samples are very dense. Although grain boundaries are difficult to be observed from the SEM images, it is clearly to see that both the samples have a "texture", which is in agreement with the XRD result (see Fig. 2(a)). However, the texture in the two samples is somewhat different. In the PbTe sample, besides many long and curly stripes, there are also many long and straight stripes. It can be seen from Fig. 2(b) that there are two groups of such straight stripes, marked by "A" and "B" in Fig. 2(b). The straight stripes in each group are parallel, whereas the orientations of the two groups are almost perpendicular to each other. In addition, there are many curly substripes accompanying some of the straight stripes, as indicated by arrows in Fig. 2(c). In the LAST-18 sample there are no above-mentioned straight stripes (see Figs. 2(d) and (e)) but curly stripes. This indicates that Ag and Sb co-doping has a significant effect on the microstructure of the PbTe materials. According to Ref. [11], the LAST-18 material is derived by isoelectronic substitution of Pb^{2+} ions for Ag^+ and Sb^{3+} in the lattice of PbTe. This generates local distortions, both structural and electronic, that are critical in determining the properties of the material. The curly stripes observed in the LAST-18 sample are probably related to the local structural distortions generated by Ag and Sb co-doping.

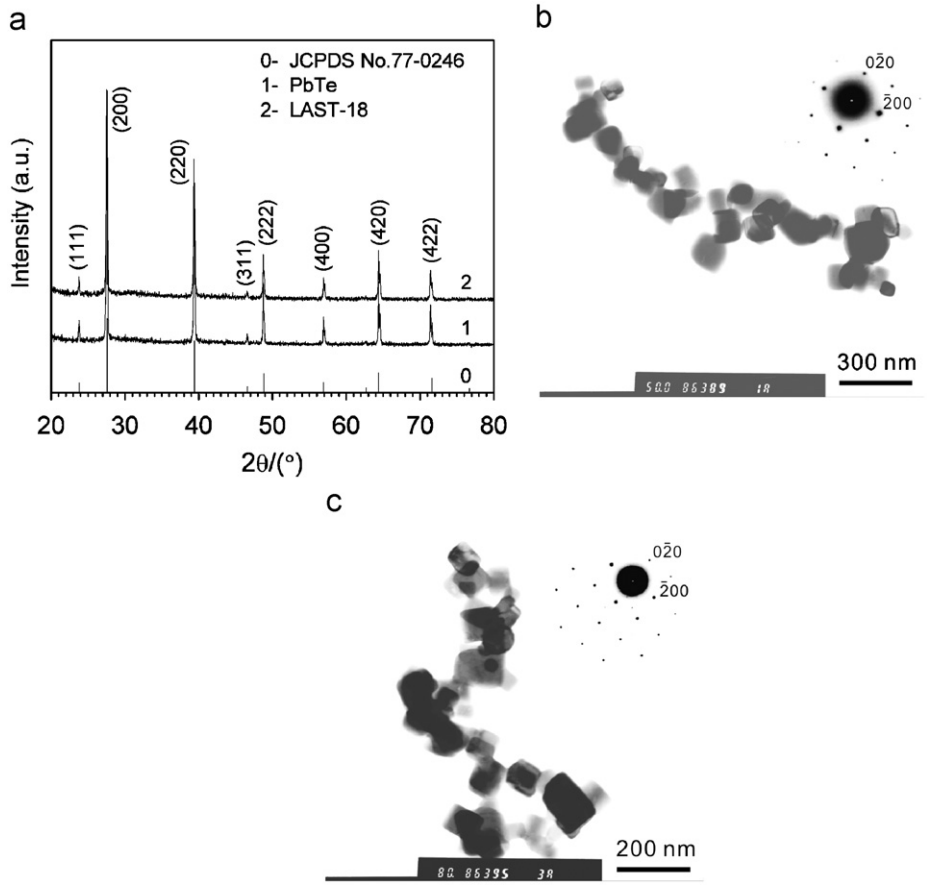

Fig. 1. (a) XRD patterns of the as-prepared PbTe and LAST-18 nanopowders, typical TEM images for (b) the PbTe and (c) the LAST-18 nanopowders.

Both the samples are brittle. The fracture surface of the PbTe sample is flatter than that of the LAST-18 sample, suggesting that the Ag and Sb co-doping can increase the fracture toughness.

As it can be seen in Table 1 that the carrier concentration of the LAST-18 sample is on the order of $10^{19}\,cm^{-3}$, while it is only on the order of $10^{17}\,cm^{-3}$ for the PbTe sample, indicating that doping Ag and Sb into PbTe markedly increases the carrier concentration. However, the carrier mobility of the LAST-18 sample is lower than that of the PbTe sample. This is because the defect concentration in the LAST-18 sample is higher due to the Ag and Sb co-doping. The mobility of the LAST-18 sample is much lower than that reported in Refs. [11,15], which should be due to different fabrication processes. The Hall coefficient changes from positive to negative after doping Ag and Sb into PbTe, indicating that the conduction changes from p- to n-type, which is in good agreement with the result of Seebeck coefficient measured at room temperature (see Fig. 3(b) in the following text).

Fig. 3(a) shows the electrical conductivity of the PbTe and LAST-18 samples as a function of temperature. Although the electrical conductivity-temperature dependence for both the samples is similar, the electrical conductivity of the LAST-18 sample is higher than that of PbTe in the whole temperature range, which can be attributed to the higher carrier concentration (see Table 1). The electrical conductivity of both the PbTe and LAST-18 samples slightly decreases with increasing temperature as $T<500\,K$, and then almost keeps constant and finally increases quickly at higher temperatures ($T>600\,K$). The decrease of electrical conductivity with increasing temperature as $T<500\,K$ is probably because the carrier mobility decreases with increasing temperature. The increase of electrical conductivity at higher temperatures ($T>550\,K$) should be due to the intrinsic excitation of carriers (electrons). The electrical conductivity of the as-prepared LAST-18 sample is higher than that reported in Ref. [16], indicating that the improvement of the process has a positive effect on the electrical conductivity. Besides the composition, the microstructure (highly dense and highly textured) of the sample should also have an important contribution to it. However, compared with the LAST-18 sample reported in Ref. [11], the as-prepared LAST-18 sample has a different electrical conductivity-temperature dependence and much lower electrical conductivity as $T<500\,K$. At room temperature the carrier concentrations for the two LAST-18 samples are similiar, while the mobility of the as-prepared LAST-18 sample is much lower (see Table 1). This indicates that the carrier scattering in the as-prepared LAST-18 sample is stronger.

XRF analysis reveals that the composition of our LAST-18 sample is $Ag_{0.9}Pb_{18}Sb_{0.58}Te_{18.99}$. The content of Ag, Sb and Te deviates from the stoichiometric composition of LAST-18. In addition, the sample is slightly contaminated by oxygen. The former is probably due to some of the chemicals (e.g. $SbCl_3$) used being very easy to be affected with damp and/or incomplete reaction during the hydrothermal reaction, and volatilization of the constituent elements during the melting. The latter could be because the LAST-18 nanopowders absorbed a lot of air at their surface, due to a large surface area, which was not fully eliminated before being sealed in a quartz tube, and thus the ingot was slightly oxidized during melting. Therefore, that the composition of the present LAST-18 sample is different from that of the LAST-18 sample in Ref. [11] could be the main reason for its lower carrier mobility.

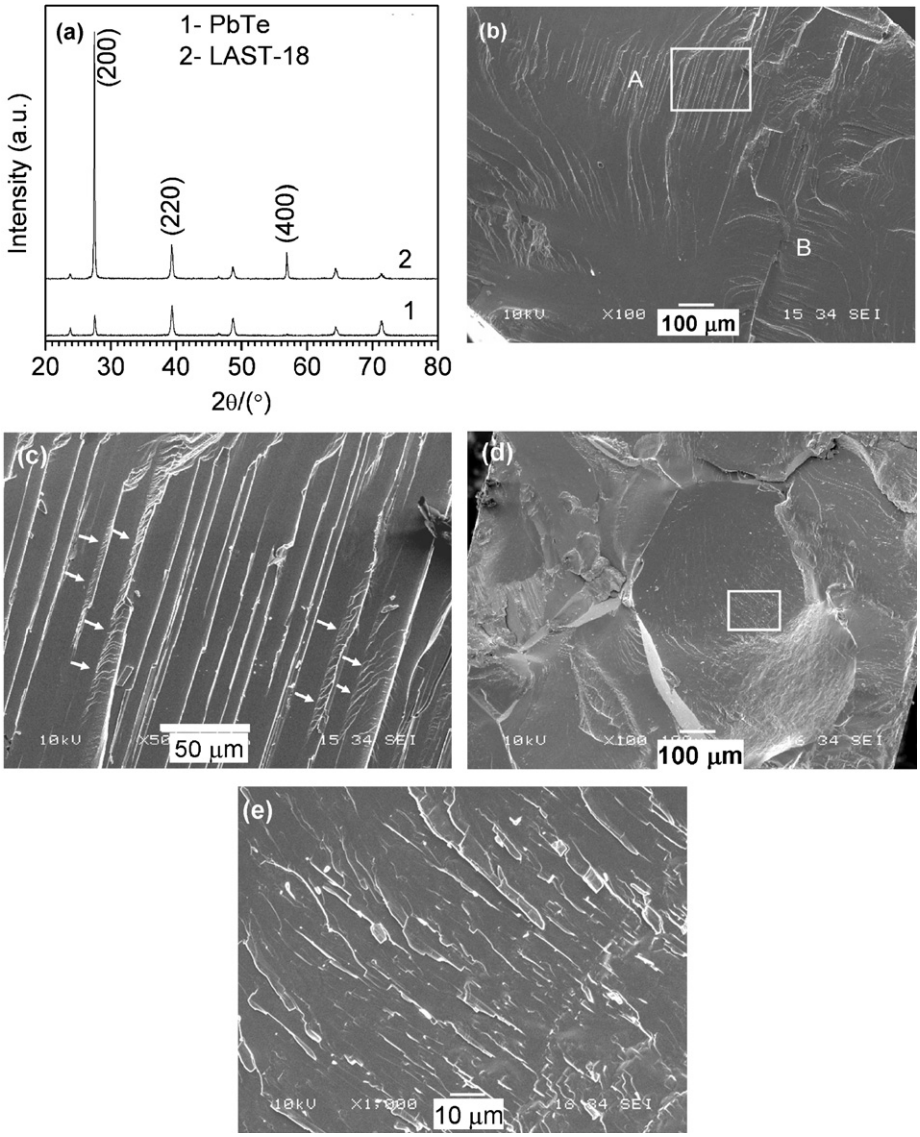

Fig. 2. (a) XRD patterns of the bulk PbTe and LAST-18 samples, and typical SEM images of the fracture surfaces of (b) the bulk PbTe and (c) enlarged image of the zone marked by a square in (b), and (d) the LAST-18 sample and (e) enlarged image of the zone marked by a square in (d).

Table 1
Room temperature carrier concentration (n), mobility (μ_H) and Hall coefficient (R_H) of the samples.

Sample	n (10^{17} cm^{-3})	μ_H (cm^2/V^1/s^1)	R_H (cm^3/C)
PbTe	9.388	386.1	6.649
LAST-18	175	105.4	−0.3567
LAST-18[a]	190	800	–

[a] The data for LAST-18 are from Ref. [11].

As it can be seen from Fig. 3(b), the Seebeck coefficient of the PbTe sample decreases dramatically when the temperature increases from 400 to 600 K and it changes from positive to negative at ~500 K. This indicates that the dominating carriers in the sample changes from holes to electrons as the temperature increases, which agrees with the result reported by Orihashi et al. [8]. The Seebeck coefficient of the LAST-18 sample is negative in the whole temperature range, indicating n-type conduction. Note that the LAST-m samples reported in Ref. [16] all have large positive Seebeck coefficients due to the samples being slightly oxidized and having a small amount of remnant Te. This indicates that the process employed in the present work efficiently eliminated the influence from both the remnant Te and oxidation. The absolute Seebeck coefficient of the LAST-18 gradually increases with increasing temperature and reaches its maximum value of 220 μV/K at 623 K and then decreases slightly with increasing temperature as $T>\sim$600 K. The decrease of the absolute Seebeck coefficient at higher temperature can be ascribed to the increase of carrier concentrations due to intrinsic excitation [17].

The temperature dependences of electrical transport properties (electrical conductivity and Seebeck coefficient) of the LAST-18 sample are very different from those reported in Ref. [11]. This must be due to different compositions and different microstructures resulted from different fabrication processes.

Fig. 3(c) shows the temperature dependence of power factor for the PbTe and LAST-18 samples, calculated from the measured electrical conductivity and Seebeck coefficient. The power factor of the PbTe sample decreases with increasing temperature as

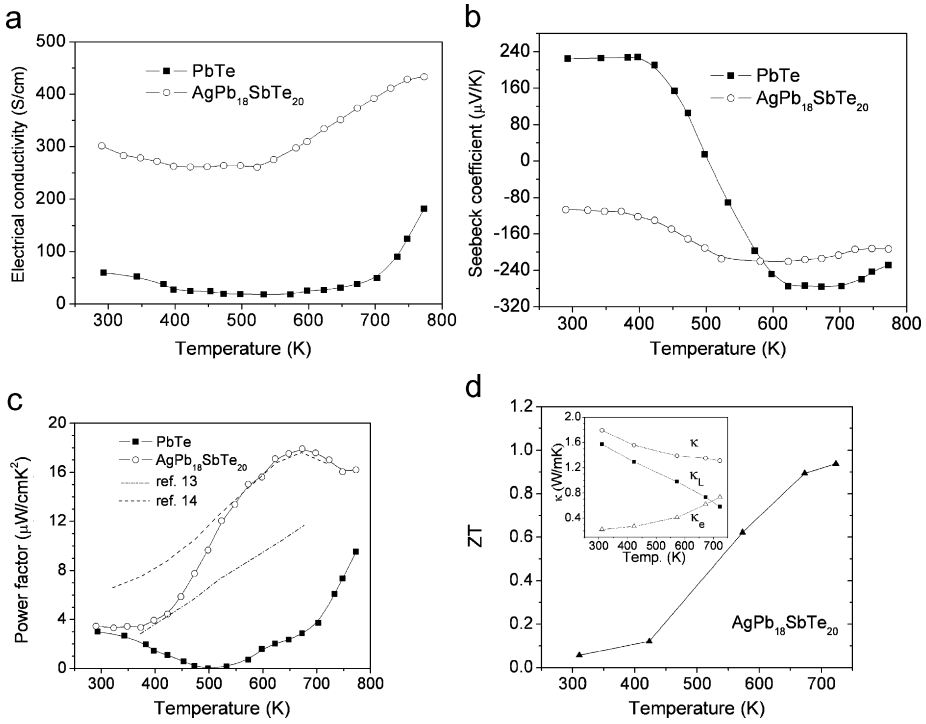

Fig. 3. Temperature dependence of (a) electrical conductivity, (b) Seebeck coefficient and (c) power factor (the results in Ref. [13,14] are also given for comparison) for the PbTe and LAST-18 samples, and (d) temperature dependence of ZT value and thermal conductivity (inset) of the LAST-18 sample.

$T<500$ K and then increases steadily above 500 K. At a given temperature, the power factor of the LAST-18 sample is higher than that of the PbTe sample in the whole temperature range measured. The maximum power factor of 17.9 $\mu W/cm^1/K^2$ is achieved at 673 K for the LAST-18 sample, which is much higher than that reported in Ref. [13] and comparable to that reported in Ref. [14]. The enhanced power factor attributes to the significant increase of the electrical conductivity without much decrease of the Seebeck coefficient.

Temperature dependence of thermal conductivity for the LAST-18 sample is shown in the inset of Fig. 3(d). Compared with the thermal conductivities, 2.8 and 3.95 W/mK^2, respectively, for 9.104×10^{-3} and 0.03 mol% PbI_2 doped n-type PbTe, at room temperature [7], the LAST-18 sample has a lower thermal conductivity. The thermal conductivity decreases monotonically with increasing temperature. At lower temperature ($T<450$ K) the thermal conductivity of the LAST-18 sample is lower than that of the LAST-18 sample reported in Ref. [11], due to much higher electrical conductivity of the latter, whereas at higher temperatures ($T>450$ K), the thermal conductivity of the LAST-18 sample is higher than that of the latter. The lattice thermal conductivity κ_l was determined by subtracting the electronic contribution κ_e as calculated using the Wiedemann–Franz law ($\kappa_e = L\sigma T$, where the Lorenz number $L\approx2.45\times10^{-8}\,W\Omega/K^2$) from the total thermal conductivity (that is, $\kappa_l=\kappa-\kappa_e$). The temperature dependences of κ_l and κ_e are also shown in the inset. As it can be seen from the inset of Fig. 3(d), the decrease of thermal conductivity with increasing temperature can be ascribed to the decrease of κ_l.

The ZT value, calculated from the Seebeck coefficient, the electrical conductivity and the thermal conductivity, as a function of temperature is shown in Fig. 3(d). For the LAST-18 sample, a high ZT value of ~0.94 is obtained at 723 K. This value is close to the maximum ZT value of 1.05 at 700 K for the unannealed $Ag_{0.8}Pb_{22.5}SbTe_{20}$ sample in Ref. [15]. Compared with the reported LAST-*m* materials, the present sample has higher thermal conductivities at high temperatures. Therefore, if we further optimize the composition, such as using Se and Sn partially substitute for Te and Pb, respectively, and adjusting the preparation conditions, such as increasing the vacuum degree before sealing the quartz tube, the TE properties of the sample should be improved, which is under way in our group.

4. Conclusions

Co-doping Ag and Sb into PbTe decreases the particle size of the hydrothermally synthesized powders and causes bulk samples with different textures. The LAST-18 sample shows n-type conduction in the whole temperature range, while a transition from p- to n-type conduction occurs at ~500 K for the PbTe sample. The electrical conductivity is markedly improved by co-doping Ag and Sb into PbTe. A ZT value of ~0.94 is obtained at 723 K for the LAST-18 sample. The approach to LAST-*m* materials presented is convenient and inexpensive.

Acknowledgments

This work was supported by Shanghai Pujiang Program and 973 Program (2007CB607500).

References

[1] F.J. DiSalvo, Science 285 (1999) 703–706.
[2] A. Majumdar, Science 303 (2004) 777–778.
[3] D.Y. Chung, T. Hogan, P. Brazis, M. Rocci-Lane, C. Kannewurf, M. Bastea, C. Uher, M.G. Kanatzidis, Science 287 (2000) 1024–1027.
[4] G.J. Snyder, E.S. Toberer, Nat. Mater. 7 (2008) 105–114.
[5] Z.H. Dughaish, Physica B 322 (2002) 205–223.
[6] T.C. Su, P.W. Zhu, H.A. Ma, G.Z. Ren, J.G. Guo, Y. Imai, X.P. Jia, J. Alloys Compd. 422 (2006) 328–331.
[7] Y. Gelbstein, Z. Dashevsky, M.P. Dariel, Physica B 363 (2005) 196–205.

[8] M. Orihashi, Y. Noda, L.D. Chen, T. Goto, T. Hirai, J. Phys. Chem. Solids 61 (2000) 919–923.
[9] K. Kishimoto, T. Koyanagi, J. Appl. Phys. 92 (2002) 2544–2549.
[10] J. Martin, G.S. Nolas, W. Zhang, L. Chen, Appl. Phys. Lett. 90 (2007) 2221121–2221123.
[11] K.F. Hsu, S. Loo, F. Guo, W. Chen, J.S. Dyck, C. Uher, T. Hogan, E.K. Polychroniadis, M.G. Kanatzidis, Science 303 (2004) 818–821.
[12] E. Quarez, K.F. Hsu, R. Pcionek, N. Frangis, E.K. Polychroniadis, M.G. Kanatzidis, J. Am. Chem. Soc. 127 (2005) 9177–9190.
[13] A. Kosuga, M. Uno, K. Kurosaki, S. Yamanaka, J. Alloys Compd. 387 (2005) 52–55.
[14] H. Wang, J.F. Li, C.W. Nan, M. Zhou, W.S. Liu, B.P. Zhang, T. Kita, Appl. Phys. Lett. 88 (2006) 092104–092106.
[15] M. Zhou, J.F. Li, T. Kita, J. Am. Chem. Soc. 130 (2008) 4527–4532.
[16] K.F. Cai, C. Yan, Z.M. He, J.L. Cui, C. Stiewe, E. Müller, H. Li, J. Alloys Compd. 469 (2009) 499–503.
[17] S.S. Kim, S. Yamamoto, T. Aizawa, J. Alloys Compd. 375 (2004) 107–113.